IETE Technical Review

ISSN: 0256-4602 (Print) 0974-5971 (Online) Journal homepage: www.tandfonline.com/journals/titr20

Impact of Graded AlGaN Buffer Layer Thickness on the DC, RF, Linearity, Intermodulation and Off-State Breakdown Characteristics of AlGaN Channel HEMT

Anupama Anand, Rakhi Narang, Dipendra Singh Rawal, Meena Mishra, Manoj Saxena & Mridula Gupta

IETE TECHNICAL REVIEW
2024, VOL. 41, NO. 5, 602–611
https://doi.org/10.1080/02564602.2024.2315628

RESEARCH ARTICLE

Impact of Graded AlGaN Buffer Layer Thickness on the DC, RF, Linearity, Intermodulation and Off-State Breakdown Characteristics of AlGaN Channel HEMT

Anupama Anand [1], Rakhi Narang [2], Dipendra Singh Rawal[3], Meena Mishra [3], Manoj Saxena [4] and Mridula Gupta [1]

[1]Department of Electronic Science, University of Delhi, New Delhi, India; [2]Sri Venkateswara College, University of Delhi, New Delhi, India; [3]Solid State Physics Laboratory, DRDO, New Delhi, India; [4]Deen Dayal Upadhyaya College, University of Delhi, New Delhi, India

ABSTRACT
This study examines the extraction of small-signal equivalent circuit parameters, linearity and intermodulation metrics, and capacitance–voltage characteristics for both AlGaN and GaN channel HEMTs. Compared to GaN channel HEMTs, AlGaN channel HEMTs have better linearity and intermodulation distortion. In the instance of AlGaN channel HEMTs, the device parasitics are decreased. Additionally, the effect of graded AlGaN buffer layer thickness on breakdown characteristics and linearity is examined. For breakdown characteristics, the 200 nm-graded AlGaN buffer layer thickness yields superior results with V_{BOff} 157 V for a thickness of 200 nm (147 V in the case of 500 nm). At 200 nm thickness, the linearity and intermodulation distortion FOMs are also reasonably good, and the remaining device properties are essentially unchanged. Hence, the graded AlGaN buffer thickness can be reduced for high-voltage applications. For higher-voltage applications, the graded AlGaN buffer thickness can, therefore, be decreased.

KEYWORDS
AlGaN channel HEMT; GaN channel HEMT; Graded AlGaN buffer; Linearity and intermodulation distortion matrices; Off-state breakdown voltage

1. INTRODUCTION

A lot of attention is paid towards designing electronic devices used in high frequency, high temperature, and high-power applications with the developed semiconductor technology. In recent years, III-Nitride-based conventional AlGaN/GaN High Electron Mobility Transistors (HEMTs) enable high temperature, high frequency, high voltage and high-power operation owing to the unique combination of physical properties, i.e. high mobility, high critical electric field, high thermal conductivity, high electron density and low on-resistance [1–5]. Due to the high critical electric field of GaN, the voltage sustainability between the drain and gate is high. The breakdown mechanism occurs due to the avalanche process near the gate edge on the gate-drain side. For high breakdown voltage applications, several AlGaN/GaN HEMTs have been designed but it is still far from GaN material limits due to many leakage paths and deficient in avalanche-withstanding capabilities [6,7]. To achieve higher breakdown voltage, the peak electric field at the gate edge of the drain-gate side should be reduced. A lot of studies have been carried out on breakdown voltage improvement using different field plate structures such as overlapping gate structures (referred to as gate field plates), source and drain field plates, 2- and 3-step field plates, slant field plates, *etc.* [8–10]. For further improvement of performance limits of GaN HEMTs in breakdown voltages and device reliability at high temperatures, AlGaN channel devices have been proposed due to their superior thermal stability and larger bandgap compared to GaN channel HEMTs [10–21]. Nanjo *et al.* reported $Al_{0.39}Ga_{0.61}N/Al_{0.16}Ga_{0.84}N$ HEMTs with the AlN buffer layer, sufficiently suppressed off-state drain leakage current which enhanced the breakdown voltage (1700V) [10]. A novel hybrid (ohmic/Schottky) drain contact with AlGaN channel HEMTS was fabricated by Zhang *et al.* and more than 2200 V breakdown voltage was obtained [13]. Wu *et al.* demonstrated Au-free AlGaN-channel HEMTs and RBHEMTs on a silicon substrate having −2 kV of V_{RB} and 2 kV of V_{FB} [14]. Raman *et al.* calculated the power figure of merits and demonstrated the AlGaN channel HEMTs' potential for microwave power and high-voltage switching applications [21]. Fabricated AlGaN channel HEMT with high mobility (807 $cm^2/V{\cdot}s$), maximum drain current 849 mA/mm and I_{ON}/I_{OFF} ratio ∼109 were reported by Xiao *et. al.* [22]. Zhang *et al.* demonstrated the first enhancement mode (E-mode) $Al_{0.05}Ga_{0.95}N$-channel p-GaN gate injection transistors with threshold voltage adjustable from 4 V to 7 V [23]. Several studies have been carried out for the high-frequency applications of AlGaN channel HEMT [24–26]. Moon *et al.* reported an extrinsic f_T of 170 GHz and f_{MAX} of 363 GHz at 50-nm gate length for graded channel AlGaN/GaN HEMT [25]. High linearity and lower intermodulation distortion at the output are essential parameters for all RF applications, especially in communication systems [27,28]. Venkatesan *et al.* reported $POIP_3$ /P_{dc} of 19.4 dB for a linearly graded channel, while the use of a square-root graded channel further improved the linearity figure of merit of a discrete device to 22.2 dB [28]. In [22], the fabricated AlGaN channel HEMT and GaN channel HEMTs have been reported with their I-V characteristics, breakdown characteristics, and an improved breakdown voltage with an increase in gate-drain distance (L_{gd}).

In this paper, the I-V characteristics were calibrated using different models and tuning the model parameters to get a good agreement between the experimental and simulated results. This paper has focused on the comparative study of linearity and intermodulation matrices, Capacitance–voltage characteristics, and small-signal equivalent circuit parameter extraction for both AlGaN and GaN channel HEMTs. In Section 2, the fabricated AlGaN channel and GaN channel HEMT device structures are described and give the workflow for the calibration of Simulation models in TCAD for both AlGaN channel and GaN channel HEMTs, as per the experimental results reported in [22]. Section 3 describes the linearity and intermodulation matrices, Capacitance–voltage characteristics, and small-signal equivalent circuit parameter extraction for both AlGaN and GaN channel HEMTs. Also, the I-V characteristics, breakdown characteristics, linearity and intermodulation matrices, Capacitance–voltage characteristics, and small-signal equivalent circuit parameter extraction for AlGaN channel HEMTs with graded AlGaN buffer layer thickness are investigated.

2. DEVICE STRUCTURE AND SIMULATION

A cross-sectional view of the device architectures *viz.* AlGaN channel HEMT and GaN channel HEMT structures are shown in Figure 1(a,b) [22]. The AlGaN/GaN HEMT structure with the same thickness of barrier layer and buffer layer with AlGaN channel HEMT, using the same device process was fabricated [22] to compare the performances of the AlGaN channel HEMT with the conventional GaN channel HEMT. The reason behind the performance difference between these HEMTs can be observed in Figure 1(c,d). The threshold voltage shift (Figure 2) is because of the difference in total fixed charge. Similar to the conventional GaN HEMT the 2DEG at heterojunction is formed by the spontaneous and piezoelectric polarization sheet charges (Figure 1(d)). Due to the

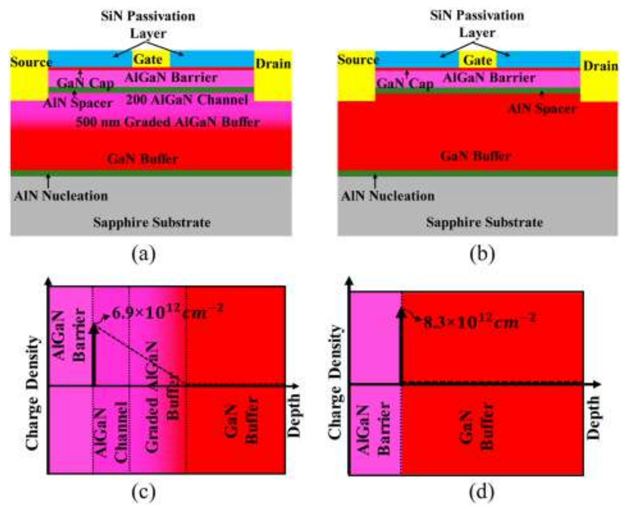

Figure 1: (a) AlGaN channel and (b) GaN channel HEMT device structures. (c) and (d) their respective charge diagrams

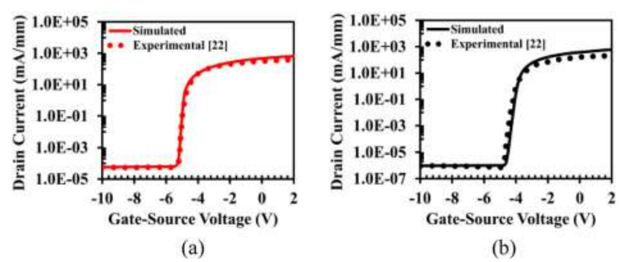

Figure 2: Comparison of experimental results with the simulated results for I_d–V_g characteristics at V_{ds} = 16 V for (a) GaN and (b) AlGaN channel HEMTs

polarization grading from the GaN to AlGaN layer, the polarization-induced charge over the graded region gets spread (Figure 1(c)), which is evenly distributed [17,29].

To calibrate the simulation model with the experimental results, reported by Xiao *et al.* in [22], iterative simulations have been performed using the TCAD ATLAS simulation tool. Models used for calibration are as follows: Shockley Read Hall Recombination (SRH), Parallel Field Dependent Mobility (FLDMOB), Hot electron injection (HEI), and Selberherr's impact ionization (IMPACT SELB). Calibration was initiated by the work function tuning of the metal–semiconductor Schottky gate to get the pinch-off voltage as reported. By defining traps and their corresponding energy levels in the bulk buffer layer (density = 1×10^{16} cm^{-3} e.level = 3.4 eV) and by tuning the interface charges, desired current densities were achieved. The interface charge values were considered as $\sim 1.3 \times 10^{13}$ cm^{-2} for AlGaN Channel HEMT and $\sim 1.1 \times 10^{13}$ cm^{-2} for GaN Channel HEMT. To reduce the error in the linear region of the output characteristics, GaN-specific field-dependent GANSAT model was

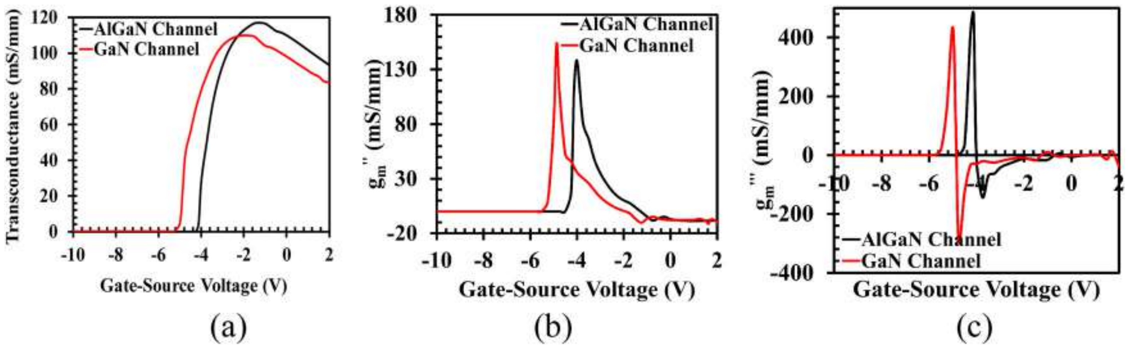

Figure 3: (a)–(c) Transconductance and second- and third-order derivatives of drain current with respect to gate bias at $V_{ds} = 16$ V for AlGaN channel (Black line) and GaN Channel (Red line) HEMTs

used, and its parameters (ann.gansat and n2n.gansat) were tuned. A comparison between the simulated and the experimental results is presented in Figure 2 in terms of I_d–V_{gs} characteristics for GaN and AlGaN channel HEMT. The comparison drawn between the calibrated result and the experimental data in Figure 2 brings forth the fact that the results are in good agreement. The simulated breakdown voltage for GaN and AlGaN channel HEMT was 119 and 147 V (Experimental Breakdown Voltage for GaN and AlGaN channel HEMT was 110 and 150 V).

3. RESULTS AND DISCUSSION

After calibration, the transconductance of AlGaN and GaN channel HEMTs was studied. Figure 3(a) represents the transconductance characteristics at $V_{ds} = 16$ V for AlGaN and GaN channel HEMTs. The peak g_m for the GaN channel was 110 mS/mm at $V_{gs} = -2.25$ V and for the AlGaN channel it was 117 mS/mm at $V_{gs} = -1.5$ V. The analysis of linearity characteristics of the device is very essential as linearity plays a significant role in RF application. To get the linearity and distortion metrics, second- and third-order derivatives ($g_m{}''$ and $g_m{}'''$) of drain current with respect to the applied gate bias are the major parameters to be considered. The mathematical equations for VIP_2, VIP_3, IIP_3 and IMD_3 [30,31] are shown by Equations (1)–(4).

$$VIP_2 = 4 \times \frac{g_m}{g''_m} \tag{1}$$

$$VIP_3 = \sqrt{24} \times \frac{g_m}{g'''_m} \tag{2}$$

$$IIP_3 = 4 \times \frac{g_m}{g'''_m \times R_s} \tag{3}$$

$$IMD_3 = \frac{9}{2} \times (VIP_3)^3 \times g'''_m \tag{4}$$

For most of the applications, $R_S = 50\ \Omega$ [32]. g''_m and g'''_m are the dominant nonlinear sources and harmonic distortion occurs due to the nonlinearity of these higher-order components. If a device has a higher value of VIP_2, VIP_3, and IIP_3 with a lower value of IMD_3, it has better linearity and lower intermodulation distortion. The Figure of Merits (FOMs) have been extracted using second- and third-order derivatives of drain current with respect to V_{gs}. It can be observed from Figure 3(b) that the g''_m shows a higher peak in GaN channel HEMT compared to AlGaN channel HEMT which corresponds to the steep slope of g_m for GaN channel HEMT. There is a sharp decrease in g''_m and becomes negative for increasing V_{gs}. This is because of the decreasing g_m with applied gate bias due to the saturated 2DEG density which limits the current to increase with applied gate voltage. As evident from Figure 3(c), a single zero crossing point in g'''_m, further results in high linearity FOMs.

A comparison of GaN channel and AlGaN channel HEMTs in terms of VIP_2, VIP_3, IIP_3 and IMD_3, respectively, is shown in Figure 4. As mentioned previously, the transconductance of GaN HEMT is marginally lower than AlGaN channel HEMT, and the lower g''_m peak for AlGaN channel HEMT results in deteriorated VIP_2. However, the overall improvement in linearity parameters i.e. VIP_3 and IIP_3 is superior in AlGaN channel HEMT, which again indicates better linearity in AlGaN channel HEMT. As evident from Figure 4(d), the IMD_3 has a lower peak at low gate bias for AlGaN channel HEMT.

The AC simulations were carried out to study the capacitances, gain and small signal parameters of the devices (AlGaN and GaN channel HEMTs). Figure 5(a,b) shows the gate–source capacitance (C_{gs}) and gate-drain capacitance (C_{gd}) for GaN channel HEMT and Figure 5(c,d) shows the gate–source capacitance and gate-drain capacitance for AlGaN channel HEMT. The trends for the C-V curve and the peak values of the gate–source capacitance (C_{gs}) and gate-drain capacitance (C_{gd}) for GaN

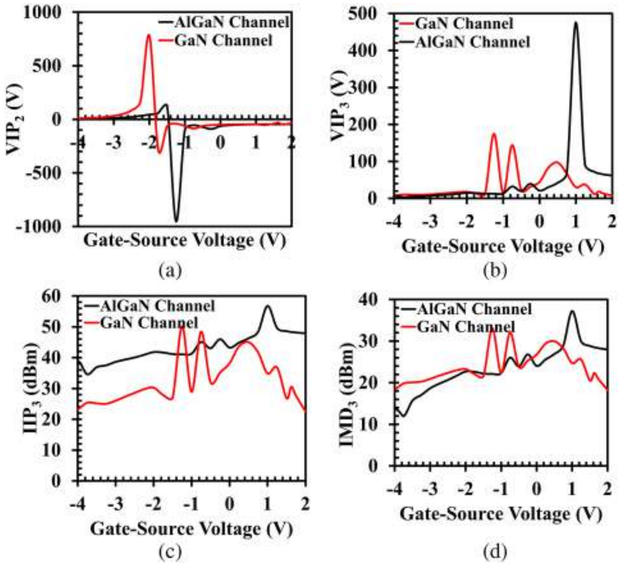

Figure 4: Comparison of GaN channel (Red Line) and AlGaN channel (Black Line) HEMTs in terms of (a) VIP_2, (b) VIP_3, (c) IIP_3 and (d) IMD_3

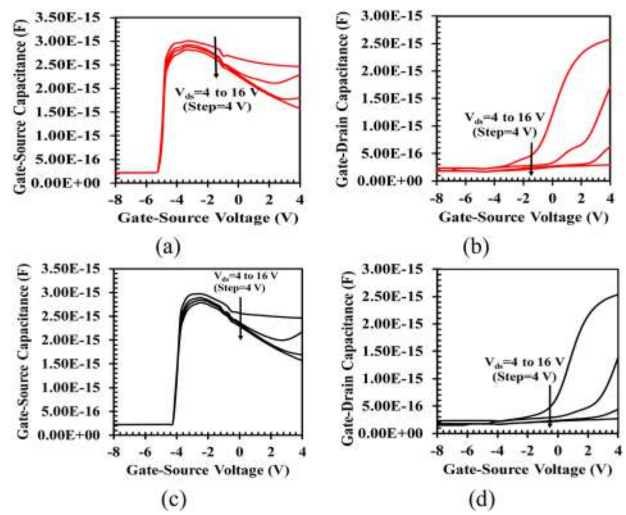

Figure 5: Gate-Source and Gate-Drain capacitances for (a)-(b) GaN channel HEMT and (c)-(d) AlGaN channel HEMT

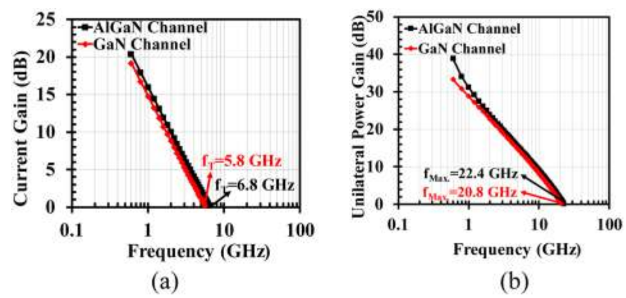

Figure 6: (a) Current Gain and (b) Unilateral Power Gain for GaN channel (Red) and AlGaN Channel (Black) HEMTs

channel and AlGaN channel HEMTs are the same. But there is a shift in gate voltage where the capacitances start increasing. The transfer characteristics have a threshold voltage shift between GaN and AlGaN channel HEMTs (Figure 2). Figure 6 shows the simulated unilateral power gain and current gain (at $V_{ds} = 10$ V) of GaN and AlGaN channel HEMTs. The f_T and $f_{Max.}$ were extracted from the current gain and unilateral power gain. The cut-off frequency (f_T) and maximum frequency ($f_{Max.}$) for AlGaN channel HEMT (6.8 and 22.4 GHz, respectively) were higher than the GaN channel HEMT (5.8 and 20.8 GHz). As shown in Figure 3, g_m is high for AlGaN channel HEMT compared to GaN channel HEMT. f_T is directly proportional to g_m and $f_{Max.}$ is directly proportional to f_T, hence the f_T and $f_{Max.}$ are high for AlGaN channel HEMT compared to GaN channel HEMT. The high gain performance of AlGaN channel HEMT enforces its suitability for high-frequency applications over GaN channel HEMT devices. The small signal equivalent circuit parameter extraction was carried out on multiple biases to compare the device parasitics of GaN and AlGaN channel HEMTs. The 10-intrinsic element small signal equivalent circuit was used for extraction. The small-signal equivalent circuit is shown in Figure 7. The conventional small-signal equivalent circuit contains the 8 (in 16-element topology)-12 (22-element topology) extrinsic elements, out of which only two extrinsic elements (Source and Drain resistance (R_s, R_d)) are considered as only these two resistances were considered during simulation [33]. The conventional extraction methodology was followed [34,35]. The initial values of the parameters were obtained from mathematical calculation and curve fitting using the simulated S-parameter data and then the equivalent circuit was designed using ADS (Advance Design System) software to optimize the value of the parameter to get a good match between the two results. Table 1 shows the comparison between the optimized small-signal equivalent circuit parameters of AlGaN and GaN channel HEMTs for different biases and after optimizing the circuit, the s-parameter from the TCAD simulation and circuit was matched, as shown in Figure 8.

After studying the linearity and intermodulation matrices, capacitance–voltage characteristics, and small-signal equivalent circuit parameter extraction for both AlGaN and GaN channel HEMTs, the focus is shifted to the impact of Graded AlGaN Buffer layer thickness on the DC, RF and Breakdown Characteristics. Also, the linearity and intermodulation and small-signal equivalent circuit parameters' dependency on Graded AlGaN buffer layer thickness are studied. Table 2 shows the variation

Table 1: Optimized small signal equivalent circuit parameters for AlGaN and GaN channel HEMTs (Frequency range 600 MHz-60 GHz)

	AlGaN Channel HEMT					
Intrinsic Elements	$V_{ds} = 10\,V$ $V_{gs} = -3\,V$	$V_{ds} = 10\,V$ $V_{gs} = -1\,V$	$V_{ds} = 15\,V$ $V_{gs} = -3\,V$	$V_{ds} = 15\,V$ $V_{gs} = -1\,V$	$V_{ds} = 20\,V$ $V_{gs} = -3\,V$	$V_{ds} = 20\,V$ $V_{gs} = -1\,V$
C_{gs} (fF)	248.55	274.78	253.73	302.58	270.41	307.03
C_{gd} (fF)	17.68	18.89	14.31	15.75	11.02	14.17
C_{ds} (fF)	6.62	6.43	6.85	6.56	7.16	6.91
R_i (Ω)	15.56	15.83	16.01	16.14	17.19	17.53
R_{gd} (Ω)	5.47	6.87	6.91	8.94	8.03	10.14
G_m (mS)	11.06	14.61	11.36	14.74	11.76	14.84
G_d (mS)	0.22	0.24	0.20	0.21	0.19	0.20
T_{au} (pSec.)	4.61	4.64	4.74	4.88	4.98	5.15
R_{gsf} (KΩ)	39.24	40.04	38.42	38.94	37.98	38.03
R_{gdf} (KΩ)	43.01	44.21	42.56	43.12	41.89	41.98
	GaN Channel HEMT					
Intrinsic Elements	$\mathbf{V_{ds} = 10\,V}$ $\mathbf{V_{gs} = -3\,V}$	$\mathbf{V_{ds} = 10\,V}$ $\mathbf{V_{gs} = -1\,V}$	$\mathbf{V_{ds} = 15\,V}$ $\mathbf{V_{gs} = -3\,V}$	$\mathbf{V_{ds} = 15\,V}$ $\mathbf{V_{gs} = -1\,V}$	$\mathbf{V_{ds} = 20\,V}$ $\mathbf{V_{gs} = -3\,V}$	$\mathbf{V_{ds} = 20\,V}$ $\mathbf{V_{gs} = -1\,V}$
C_{gs} (fF)	265.22	300.91	305.26	338.42	325.26	356.20
C_{gd} (fF)	20.17	22.53	15.60	20.40	15.47	17.25
C_{ds} (fF)	7.69	7.54	8.96	8.13	9.01	8.67
R_i (Ω)	14.33	15.51	14.77	15.99	15.03	16.25
R_{gd} (Ω)	6.59	9.12	8.09	10.79	9.81	10.93
G_m (mS)	9.73	13.95	10.08	14.01	10.43	14.15
G_d (mS)	0.20	0.25	0.19	0.27	0.16	0.25
T_{au} (pSec.)	6.22	5.54	7.57	5.81	7.84	6.08
R_{gsf} (KΩ)	28.03	28.48	27.86	28.13	27.11	27.96
R_{gdf} (KΩ)	22.17	22.58	21.79	22.01	21.03	21.89

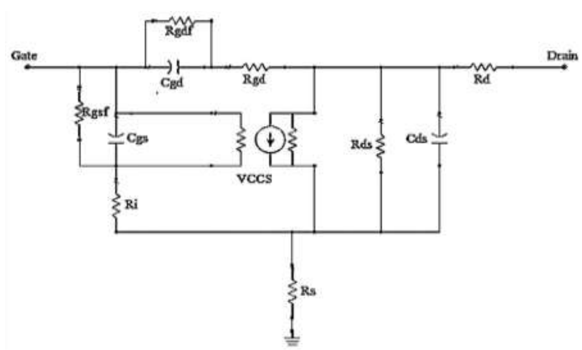

Figure 7: Small-signal equivalent circuit with ten intrinsic elements

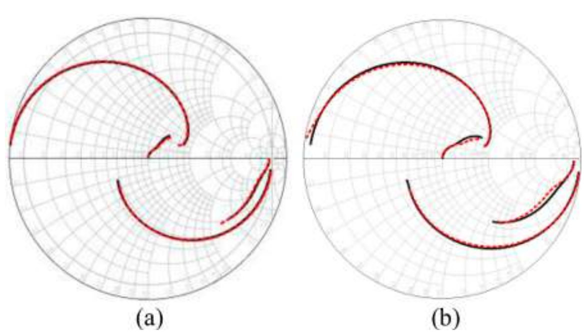

Figure 8: S-parameter from ATLAS simulation (Red) and its circuit simulation in ADS (Black) for (a) AlGaN channel HEMT and (b) GaN channel HEMT at $V_{ds} = 10\,V$ and $V_{gs} = -1\,V$

in graded AlGaN buffer layer thickness used for investigation using TCAD simulations. The graded AlGaN buffer layer thickness is varied from 200 nm to 700 nm in step of 100 nm out of which 500 nm is the experimental structure in [27]. The GaN buffer layer thickness is adjusted relatively so that the overall thickness of the buffer layer is maintained. The required simulations were performed for different dimensions mentioned in Table 2. The DC simulation provided the Drain current vs. applied gate bias and using it, the second and third derivatives of change in drain current with applied gate bias werederived. Using Equations (1)–(4), different linearity and intermodulation distortion matrices were extracted for different graded AlGaN buffer layer thicknesses. Figure 9(a–c) shows the first-order, second-order and third-order derivatives of Drain current with applied gate bias at $V_{ds} = 16\,V$ for different Graded AlGaN buffer layer thickness. The g_m for all the graded AlGaN buffer layer thicknesses is overlapped with each other. The drain current had very slight variation; hence the first -order derivative of the drain current is almost overlapping, but the second- and third-order derivatives are varying with thickness which will further affect the linearity and intermodulation distortion FOMs. Figure 10(a–d) shows the linearity and intermodulation distortion FOMs VIP_2, VIP_3, IIP_3 and IMD_3 for different Graded AlGaN buffer layer thicknesses. It is observed that for graded AlGaN buffer thickness of

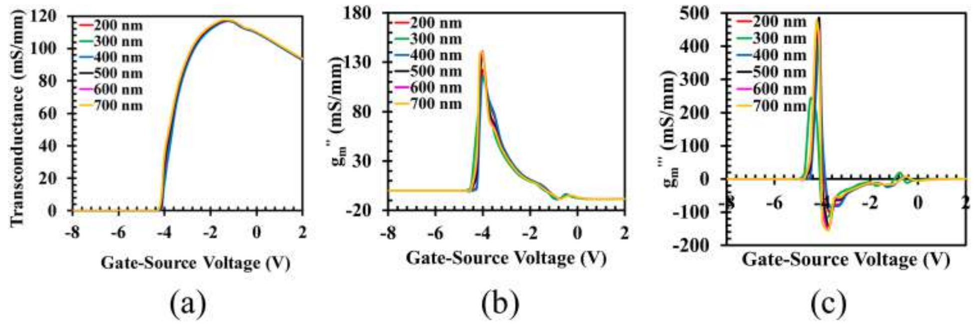

Figure 9: (a) first-order, (b) second-order and (c) third-order derivatives of Drain current with applied gate bias at $V_{ds} = 16$ V for different Graded AlGaN buffer layer thickness

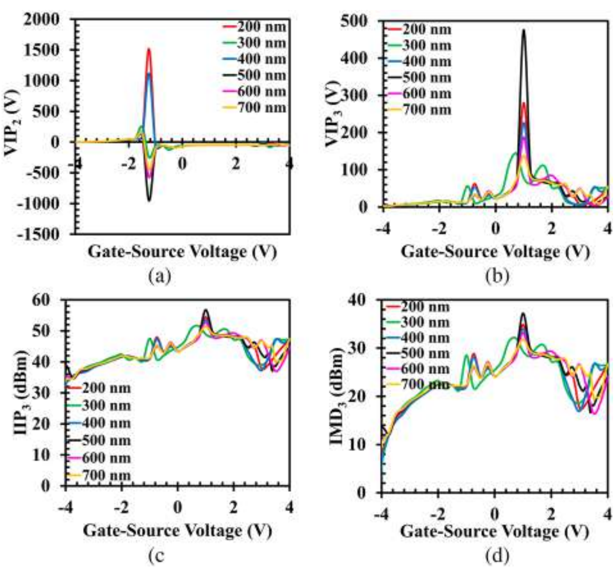

Figure 10: Linearity and intermodulation distortion FOMs *viz*. (a) VIP_2, (b) VIP_3, (c) IIP_3 and (d) IMD_3 for different Graded AlGaN buffer layer thicknesses

Table 2: Variation of graded algan buffer layer thickness for TCAD simulations

Graded AlGaN Buffer Thickness (nm)	200	300	400	500	600	700
GaN Buffer Thickness (µm)	1.3	1.2	1.1	1.0	0.9	0.8

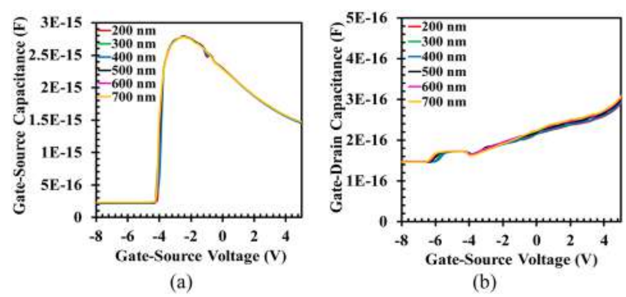

Figure 11: (a) Gate-Source capacitance (b) Gate-Drain capacitance for different Graded AlGaN buffer layer thickness

Table 3: Optimized small signal equivalent circuit parameters for different graded AlGaN buffer layer thickness HEMTs at $V_{ds} = 10$ V and $V_{gs} = -1$ V (Frequency range 600 MHz–60 GHz)

Intrinsic Parameters	200 nm	300 nm	400 nm	500 nm	600 nm	700 nm
C_{gs} (fF)	295.91	292.57	291.46	274.78	293.68	298.13
C_{gd} (fF)	19.16	18.93	18.49	18.89	18.05	19.56
C_{ds} (fF)	4.09	4.56	4.86	2.18	5.78	5.32
R_i (Ω)	18.36	20.77	17.60	17.22	17.15	17.09
R_{gd} (Ω)	6.15	4.44	3.80	4.87	4.66	6.16
G_m (mS)	14.26	14.50	14.63	14.61	14.76	14.78
G_d (mS)	0.32	0.30	0.29	0.25	0.25	0.24
T_{au} (pSec.)	4.61	4.54	4.54	4.339	4.54	4.54
R_{gsf} (KΩ)	39.79	39.50	39.35	40.04	41.91	41.34
R_{gdf} (KΩ)	42.41	42.72	43.53	44.21	42.86	43.19

200 nm, the VIP_2 and IIP_3 have higher values compared to the other thicknesses. In Figure 10(c), the IIP_3 peak at $V_{gs} = -0.75$ V, 200 nm shows the highest peak. But the peak VIP_3 value is achieved for 500 nm thickness and the second peak is achieved for 200 nm thickness. Also, the IMD_3 peaks (at $V_{gs} = 1$ V) are lower for 200 nm thickness than 500 nm. The AC simulations were carried out to study the impact of graded AlGaN buffer layer thickness on gate–source capacitance and gate-drain capacitance. Figure 11(a,b) shows the gate–source capacitance and gate-drain capacitance, respectively for different Graded AlGaN buffer layer thicknesses. It is evident from Figure 11 that the different graded AlGaN buffer layer thicknesses have overlapping capacitance behavior. Then the small-signal equivalent circuit parameter extraction was investigated for multiple biases. Table 3 shows the optimized intrinsic parameters for different graded AlGaN buffer layer thicknesses. After optimizing the circuit, the s-parameter from the TCAD simulation and circuit were matched, as shown in Figure 12 for different graded AlGaN buffer layer thicknesses. The intrinsic parameters have small differences as the DC and capacitance characteristics vary slightly. As a result, the f_T and $f_{Max.}$ have a negligible change.

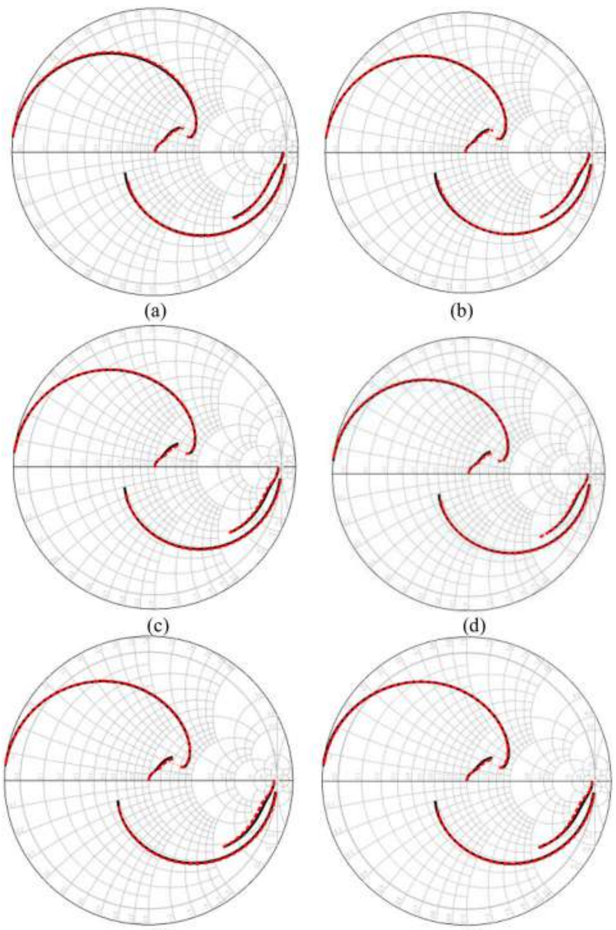

Figure 12: S-parameter from ATLAS simulation (Red) and its circuit simulation in ADS (Black) for (a) 200 nm, (b) 300 nm, (c) 400 nm, (d) 500 nm, (e) 600 nm and (f) 700 nm graded AlGaN buffer layer thickness at $V_{ds} = 10$ V and $V_{gs} = -1$ V

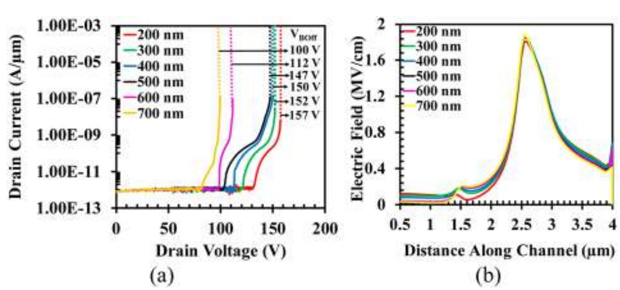

Figure 13: (a) Off-state Breakdown Characteristics and (b) Electric-Field along the channel length at $V_{gs} = -10$ V and $V_{ds} = 80$ V for different Graded AlGaN buffer layer thicknesses

Then the off-state breakdown characteristics for different buffer layer thicknesses were investigated. Figure 13(a) shows the off-state breakdown characteristics at $V_{gs} = -10$ V. Figure 13(b) shows the electric field along the channel length at $V_{gs} = -10$ V and $V_{ds} = 80$ V for different Graded AlGaN buffer layer thickness. The off-state breakdown behavior shows a great impact for the graded AlGaN buffer thickness variation. The 200 nm shows the highest breakdown of 157 V. As the graded AlGaN buffer layer thickness is reduced from 700 to 200 nm, the breakdown is increasing. For 300 and 400 nm thickness, the breakdown voltage has a difference of only 2 V as is evident from the electric field plot in which the electric field peaks are overlapped for 300 and 400 nm. And the 200 nm thickness buffer layer has the lowest electric field peak. Hence the breakdown voltage is highest (157 V) for a 200 nm thick-graded AlGaN buffer layer.

4. CONCLUSION

For both AlGaN and GaN channel HEMTs, the extraction of small-signal equivalent circuit parameters, as well as linearity and intermodulation metrics, have been studied. AlGaN channel HEMTs perform better than GaN channel HEMTs in terms of linearity and intermodulation distortion. Meanwhile, in the case of AlGaN channel HEMTs, the device parasitics were also decreased. Additionally, the effect of AlGaN buffer layer thickness on breakdown characteristics and linearity is examined. Better breakdown properties are shown by the 200 nm graded AlGaN buffer layer thickness. V_{BOff} was raised from 147 V (in the case of 500 nm) to 157 V for a thickness of 200 nm. While the remaining device parameters (capacitances, f_T, f_{Max}, small-signal equivalent circuit parameters) are almost the same, the linearity and intermodulation distortion FOMs for 200 nm buffer thickness are likewise comparably as excellent as 500 nm thickness. Therefore, it is possible to minimize the graded AlGaN buffer thickness for applications requiring high-voltage and -power.

ACKNOWLEDGEMENTS

The authors thank the Department of Electronic Science, University of Delhi; Solid State Physics Laboratory, Ministry of Defence, DRDO CARS project Ref. No.:1115/TS/SPL/CARS-95/2022; DBT STAR College Laboratory at Deen Dayal Upadhyaya College, University of Delhi; University of Delhi IoE Grant Ref. No.: IoE-DU/MRP/2022/056 and Department of Science and Technology project Ref. No.: SPG/2021/003067 for providing necessary tools and financial assistance for the completion of this work.

DISCLOSURE STATEMENT

No potential conflict of interest was reported by the author(s).

FUNDING

This work was supported by Solid State Physics Laboratory, Ministry of Defence, DRDO CARS project [grant number 1115/TS/SPL/CARS-95/2022]; DBT STAR College Laboratory at Deen Dayal Upadhyaya College, University of

Delhi; University of Delhi IoE Grant [grant number IoE-DU/MRP/2022/056]; Department of Science and Technology project [grant number SPG/2021/003067].

ORCID

Anupama Anand http://orcid.org/0000-0002-8986-7748
Rakhi Narang http://orcid.org/0000-0001-6225-7176
Meena Mishra http://orcid.org/0000-0002-8090-483X
Manoj Saxena http://orcid.org/0000-0002-9368-4194
Mridula Gupta http://orcid.org/0000-0002-6994-6828

REFERENCES

1. M. E. Levinshtein, S. L. Rumyantsev, and M. S. Shur. *Properties of Advanced Semiconductor Materials: GaN, AIN, InN, BN, SiC, SiGe*. Canada: John Wiley & Sons, 2001.
2. B. Mounika, J. Ajayan, S. Bhattacharya, and D. Nirmal, "Recent developments in materials, architectures and processing of AlGaN/GaN HEMTs for future RF and power electronic applications: A critical review," *Micro Nanostruct.*, Vol. 168, p. 207317, 2022.
3. J. P. Kozak, *et al.*, "Stability, reliability, and robustness of GaN power devices: A review," *IEEE Trans. Power Electron.*, Vol. 38, no. 7, pp. 8442–71, 2023.
4. J. Ajayan, D. Nirmal, P. Mohankumar, B. Mounika, S. Bhattacharya, S. Tayal, and A. S. A. Fletcher, "Challenges in material processing and reliability issues in AlGaN/GaN HEMTs on silicon wafers for future RF power electronics & switching applications: A critical review," *Mater. Sci. Semicond. Process.*, Vol. 151, no. 7, p. 106982, Nov. 2022.
5. R. Sun, J. Lai, W. Chen, and B. Zhang, "Gan power integration for high frequency and high efficiency power applications: A review," *IEEE. Access.*, Vol. 8, pp. 15529–42, 2020.
6. Y.-H. Chang, J.-J. Wang, and G.-L. Shen, "Improving off-state breakdown voltage of a double-channel AlGaN/GaN HEMT with air-bridge field plate and slant field plate," *Solid State Electron. Lett.*, Vol. 2, pp. 92–7, 2020.
7. G. Sheu, Y.-L. Song, R. Mogarala, D. Susmitha, and K. Issac, "Breakdown behavior of metal contact positions in GaN HEMT with nitrogen-implanted gate using TCAD simulation," *Micromachines*, Vol. 13, no. 2, p. 169, 2022.
8. S. Karmalkar, and U. K. Mishra, "Enhancement of breakdown voltage in AlGaN/GaN high electron mobility transistors using a field plate," *IEEE Trans. Electron Devices*, Vol. 48, no. 8, pp. 1515–21, 2001.
9. J. Wong, "Novel asymmetric slant field plate technology for high-speed low-dynamic R on E/D-mode GaN HEMTs," *IEEE Electron Device Lett.*, Vol. 38, no. 1, pp. 95–8, 2016.
10. Neha, V. Kumari, M. Gupta, and M. Saxena, "Investigation of proton irradiated dual field plate AlGaN/GaN HEMTs: TCAD based assessment," *Microelectron. J.*, Vol. 122, pp. 105405, 2022.
11. T. Nanjo, *et al.*, "Algan channel HEMT with extremely high breakdown voltage," *IEEE Trans. Electron Devices*, Vol. 60, no. 3, pp. 1046–53, 2013.
12. M. Ghaffari, and A. A. Orouji, "Dual trench AlGaN/GaN HEMT on SiC substrate: A novel device to improve the breakdown voltage and high power performance," *Physica E.*, Vol. 80, no. 7, pp. 108–14, 2016.
13. W. Zhang, J. Zhang, M. Xiao, L. Zhang, and Y. Hao, "High breakdown-voltage (> 2200 V) AlGaN-channel HEMTs with ohmic/Schottky hybrid drains," *IEEE J. Electron Devices Soc.*, Vol. 6, pp. 931–5, 2018.
14. Y. Wu, *et al.*, "Au-Free $Al_{0.4}Ga_{0.6}N$ /$Al_{0.1}Ga_{0.9}N$ HEMTs on silicon substrate with high reverse blocking voltage of 2 kV," *IEEE Trans. Electron Devices*, Vol. 68, no. 9, pp. 4543–9, 2021.
15. A. G. Baca, *et al.*, "RF performance of $Al_{0.85}Ga_{0.15}N/Al_{0.7}Ga_{0.3}N$ high electron mobility transistors with 80-nm gates," *IEEE Electron Device Lett.*, Vol. 40, no. 1, pp. 17–20, 2018.
16. Y. Wu, *et al.*, "More than 3000 V reverse blocking Schottky-drain AlGaN-channel HEMTs with > 230 MW/cm 2 power figure-of-merit," *IEEE Electron Device Lett.*, Vol. 40, no. 11, pp. 1724–7, 2019.
17. N. Venkatesan, J.-S. Moon, and P. Fay, "Electric field engineering in graded-channel GaN-based HEMTs," in 2021 IEEE BiCMOS and compound semiconductor integrated circuits and technology symposium (BCICTS), Monterey, CA, USA, 2021, pp. 1–4. IEEE.
18. C.-S. Lee, C.-L. Li, W.-C. Hsu, C.-Y. You, and H.-Y. Liu, "Enhancement-mode characteristics of $Al_{0.65}Ga_{0.35}N$/ $Al_{0.3}Ga_{0.7}N$ /AlN/SiC MOS-HFETs," *IEEE J Electron Devices Soc.*, Vol. 9, pp. 1003–8, 2021.
19. H. Xue, *et al.*, "$Al_{0.65}Ga_{0.35}N/Al_{0.4}Ga_{0.6}N$ micro-channel heterojunction field-effect transistors with current density over 900 mA/mm," *IEEE Electron Device Lett.*, Vol. 41, no. 5, pp. 677–80, 2020.
20. B. Chatterjee, *et al.*, "Interdependence of electronic and thermal transport in AlxGa1-xN channel HEMTs," *IEEE Electron Device Lett.*, Vol. 41, no. 3, pp. 461–4, 2020.
21. A. Raman, S. Dasgupta, S. Rajan, J. S. Speck, and U. K. Mishra, "Algan channel high electron mobility transistors: Device performance and power-switching figure of merit," *Jpn. J. Appl. Phys.*, Vol. 47, no. 5R, p. 3359, 2008.
22. M. Xiao, J. Zhang, X. Duan, W. Zhang, H. Shan, J. Ning, and Y. Hao, "High performance $Al_{0.1}Ga_{0.9}N$ channel HEMTs," *IEEE Electron Device Lett.*, Vol. 39, no. 8, pp. 1149–51, 2018.

23. L. Zhang, *et al.*, "AlGaN-channel gate injection transistor on silicon substrate with adjustable 4–7 V threshold voltage and 1.3 kV breakdown voltage," *IEEE Electron Device Lett.*, Vol. 39, no. 7, pp. 1026–9, 2018.

24. S. Bajaj, *et al.*, "Graded AlGaN channel transistors for improved current and power gain linearity," *IEEE Trans. Electron Devices*, Vol. 64, no. 8, pp. 3114–9, 2017.

25. J.-S. Moon, *et al.*, "360 GHz fMAX graded-channel AlGaN/GaN HEMTs for mmW low-noise applications," *IEEE Electron Device Lett.*, Vol. 41, no. 8, pp. 1173–6, 2020.

26. J.-S. Moon, *et al.*, "Power scaling of graded-channel GaN HEMTs with mini-field-plate T-gate and 156 GHz fT," *IEEE Electron Device Lett.*, Vol. 42, no. 6, pp. 796–9, 2021.

27. N. Venkatesan, *et al.*, "RF performance of GaN-based graded-channel HEMTs," in 2020 IEEE BiCMOS and Compound Semiconductor Integrated Circuits and Technology Symposium (BCICTS), Monterey, CA, USA, 2020, pp. 1–4, IEEE.

28. N. Venkatesan, G. Silva-Oelker, and P. Fay, "Graded-channel GaN-based HEMTs for high linearity amplifiers at millimeter-wave," in 2019 IEEE BiCMOS and Compound Semiconductor Integrated Circuits and Technology Symposium (BCICTS), Nashville, TN, USA, 2019, pp. 1–4, IEEE.

29. P. Sung Park, D. N. Nath, S. Krishnamoorthy, and S. Rajan, "Electron gas dimensionality engineering in AlGaN/GaN high electron mobility transistors using polarization," *Appl. Phys. Lett.*, Vol. 100, no. 6, pp. 063507, 2012.

30. S. Kang, B. Choi, and B. Kim, "Linearity analysis of CMOS for RF application," *IEEE Trans. Microwave Theory Tech.*, Vol. 51, no. 3, pp. 972–7, 2003.

31. M. Rao, R. Ranjan, and N. Kashyap, "Performance analysis of normally-on dual gate AlGaN/GaN HEMT," *Trans. Electric. Electron. Mater.*, Vol. 22, pp. 691–9, 2021.

32. S. Jaghargh, S. Sadaf, and A. A. Orouji, "An AlGaN/GaN HEMT by the periodic pits in the buffer layer," *Phys. Scr.*, Vol. 94, no. 10, pp. 105002, 2019.

33. A. Anand, *et al.*, "A comparative study on the accuracy of small-signal equivalent circuit modeling for large gate periphery GaN HEMT with different source to drain length and gate width," *Microelectron. J.*, Vol. 118, pp. 105258, 2021.

34. G. Dambrine, A. Cappy, F. Heliodore, and E. Playez, "A new method for determining the FET small-signal equivalent circuit," *IEEE Trans. Microwave Theory Tech.*, Vol. 36, no. 7, pp. 1151–9, 1988.

35. A. Jarndal, and G. Kompa, "A new small signal model parameter extraction method applied to GaN devices," in IEEE MTT-S International Microwave Symposium Digest, San Francisco, CA, USA, 2005, pp. 1423.6, IEEE, 2005.

AUTHORS

Anupama Anand (Student Member, IEEE) received her BSc in electronic science from BRABU in 2016 and an MSc in electronic science from Delhi University in 2018. She is currently working as a research scholar at the Department of Electronic Science, University of Delhi South Campus. She is also associated with Solid State Physics Laboratory, DRDO as a senior research fellow. Her research interests include simulation and RF modeling of GaN HEMT devices.

Email: anupama113anand@gmail.com

Rakhi Narang (Senior Member, IEEE) received the BSc, MSc, and PhD degrees in electronics from the University of Delhi, New Delhi, India, in 2005, 2007, and 2014, respectively. She is currently an assistant professor with the Department of Electronics, Sri Venkateswara College, University of Delhi. She is also associated with the semiconductor device research laboratory, Department of Electronic Science, University of Delhi South campus. She has authored/coauthored 75 technical papers in various international journals and conference proceedings.

E-mail: rnarang@svc.ac.in

Dipendra Singh Rawal (Member, IEEE) received an MSc degree in physics and MTech degree in electronics and communication engineering from IIT Roorkee, Roorkee, India, in 1988 and 1990, respectively, and the PhD degree in physics from IIT Delhi, New Delhi, India, in 2012. He is currently the associate director (Sc. "H") of Solid State Physics Laboratory, DRDO, New Delhi, India where he is involved in the development of GaN high electron mobility transistor based monolithic microwave integrated circuit technology. He has published more than 60 research papers in various international journals and conferences.

Email: dsrawal15@gmail.com

Meena Mishra (Member, IEEE) received the BSc andMSc degrees from Delhi University, in 1986 and 1988, respectively, and the PhD degree from Jamia Millia Islamia University, New Delhi, in 2006, all in electronics. She is currently the director (Sc. "H") of the Solid State Physics Laboratory, DRDO. She was involved in designing high-frequency GaAs-based digital integrated circuits. She is currently involved in GaN microwave FET and GaAs MMlC research and development projects.

E-mail: mishra.meena.sspl@gov.in

Manoj Saxena received MSc and PhD in electronics from the University of Delhi, New Delhi, in 2000 and 2006 respectively. He is currently a professor in the Department of Electronics, Deen Dayal Upadhyaya College, University of Delhi, New Delhi, India. He has authored or co-authored 360 technical papers in international journals (130 Scopus Indexed) and conference proceedings and delivered 40+ EDS distinguished lectures. His research areas are mathematical modeling and TCAD simulation of non-classical MOSFET, tunnel FET, and HEMT designs and has reviewed 280+ manuscripts for 40+ leading international journals. He is a Fellow of the National Academy of Sciences India a Fellow-The Institution of Electronics and Telecommunication Engineers (IETE), India, and the Optical Society of India, Senior Member-IEEE, Member of the Institute of Physics (UK), and Member of Institution of Engineering and Technology (IET), UK. In past he has served IEEE in different capacities *i.e.* Vice-Chair- IEEE EDS SRC Region 10 (2015-2017); Secretary - IEEE Delhi Section (2019; EDS Newsletter Regional Editor of South East Asia (2015-2020); Member of the IEEE EDS Board of Governor (2018-2021, 2021-2023); Associate Editor-in-Chief of the IEEE EDS Newsletter (2021-2023). He is IEEE EDS Distinguished Lecturer (2016-) and Chairman of the EDS Delhi Chapter (2022 -).

E-mail: msaxena@ddu.du.ac.in

Mridula Gupta (Senior Member, IEEE) received PhD degree in optoelectronics from the University of Delhi, India, in 1998. Since 1989, she has been with the Department of Electronic Science, University of Delhi South Campus, India, and is currently a senior professor. She has authored or coauthored more than 395 publications in international and national journals and conference proceedings. Her current research interests include modeling and simulation of MOSFETs, MESFETs, and HEMTs, for microwave applications and TFET for biosensing applications. She is a Senior Member of IEEE, a Fellow of IETE and a Former chairperson of IEEE EDS Delhi Chapter.

Corresponding author. Email: mridula@south.du.ac.in